GP Method: A Hybrid Approach to Broadband Ground Motion Simulation

Robert Graves (rwgraves@usgs.gov) U.S. Geological Survey, Pasadena, CA, USA

Arben Pitarka (pitarka1@llnl.gov) Lawrence Livermore National Laboratory, Livermore, CA, USA

Release Notes (V. 19.4)

- Kinematic Rupture Generator (genslip-v5.4.1):

Revised computation of rupture time perturbations (Δt parameter in equation A5 of Graves and Pitarka, 2016) to reduce strength of magnitude scaling (following Wirth et al., 2017). New relation is

$$\Delta t = b_0 + b_1 M_o^{1/3}$$

with $b_0 = -0.1$ and $b_1 = -5.0\times10^{-8}$ set as defaults.

- High Frequency Simulation Code (hb_high_v6.0.0):

Revised determination of "Frankel" corner-frequency adjustment factor based on Boore (2009). The parameter "bigC" is now computed directly as the square of the ratio of the subevent corner frequency and the main event corner frequency. This new formulation removes the dependence of the main event corner frequency on subevent moment that was part of the Frankel (1995) formulation, which then made the scaling slightly dependent of choice of subevent dimension. The new formulation removes this dependence.

- Near Surface Velocity Structure (V_{S30ref}=500 m/s):

All 1D velocity structures used for active tectonic regions have been updated and modified to have a reference V_{s30} of 500 m/s. These updated velocity structures are used in both the calculation of Green's functions for the low-frequency computation and as input to the high-frequency stochastic computation. This V_{s30} of 500 m/s is the V_{ref} that is input to the match filtering code in the simulation pipeline. The change to V_{s30} of 500 m/s from the previous value of 863 m/s was done for two primary reasons. First, the previous velocity profiles with higher reference V_{s30} effectively double-counted impedance amplification effects because the deeper velocity structure had a slower gradient that was not consistent with the hard-rock near surface material. Second, the use of a lower reference V_{s30} of 500 m/s means that the adjustments made to site-specific V_{s30} values will generally be much less severe since the 500 m/s reference value is closer to most site-specific values.

Method Overview

Our broadband ground motion simulation procedure is a hybrid technique that computes the low frequency and high frequency ranges separately and then combines the two to produce a single time history (Figure 1). At frequencies below 1 Hz, the methodology is deterministic and contains a theoretically rigorous representation of fault rupture and wave propagation effects, and attempts to reproduce recorded ground motion waveforms and amplitudes. At frequencies above 1 Hz, it uses a stochastic representation of source radiation, which is combined with a simplified theoretical representation of wave propagation and scattering effects. The use of different simulation approaches for the different frequency bands results from the seismological observation that source radiation and wave propagation effects tend to become stochastic at frequencies of about 1 Hz and higher, primarily reflecting our relative lack of knowledge about the details of these phenomena at higher frequencies. Recent variations of the hybrid approach include the work of Liu et al (2006) and Frankel (2009).

Other features of our methodology are guided by studies that examine the depth-dependency of key rupture properties (e.g., Mikumo, 1992; Scholz, 2002). Observations from recent earthquakes show that shallow rupturing events generate relatively weak high frequency ground motions compared to deeper ruptures (Kagawa et al., 2004; Shearer et al., 2006; Pitarka et al., 2009). This type of behavior can be explained by velocity strengthening friction during fault rupture at shallow depths. During the rupture process, this leads to a reduction of rupture propagation speed and a lengthening of the rise time in these relatively weak zones of the fault. For large earthquakes, it has also been suggested that a similar transition region exists along the bottom edge of the fault where the rupture progresses from an unstable to stable sliding mode as it crosses the brittle to ductile transition in the lower crust (e.g., Hillers and Wesnousky, 2008).

Our kinematic rupture generator uses variable spatial and temporal kinematic rupture parameters that are calibrated using recorded ground motion and observed rupture kinematics. The rupture generation process begins with the specification of a random slip field that is filtered to have a roughly wavenumber-squared falloff (e.g., Mai and Beroza, 2002). The slip values are scaled to have a coefficient of variation of 0.75 and to also match the desired seismic moment. Given a prescribed hypocenter, the rupture propagation times across the fault are determined such that the average rupture speed scales at about 80% of the local shear wave velocity. The rupture speed is further reduced by a factor of 0.6 for depths of 5 km and less, which is designed to represent the shallow, weak zone in surface-rupturing events. A perturbation is then applied to the rupture time at each subfault that is partially correlated with local slip such that the rupture tends to propagate faster in regions of large slip and slows down in regions of low slip. The slip-rate function is a Kostrov-like pulse (Liu et al., 2006) with a total duration (rise time) that is partially correlated with the square root of the local slip. Additionally, the rise time is scaled up by a factor of two within the 0–5 km depth range. The average rise time across the fault is constrained to scale in a self-similar manner with the seismic moment (Somerville et al., 1999). A complete description of the rupture generator can be found in Graves and Pitarka (2016).

Our methodology also incorporates the use of frequency-dependent non-linear site amplification factors based on V_{s30} classification, and as implemented in the GMPEs of Boore et al. (2014) and Campbell and Bozorgnia (2014). The use of V_{s30} is attractive because this parameter is readily available for most regions and the amplification functions are easy to compute and apply to large-scale simulations. The main drawbacks to the V_{s30} approach are the potential omission of detailed site-specific information about the soil column and the lack of phase modification in the resulting waveform.

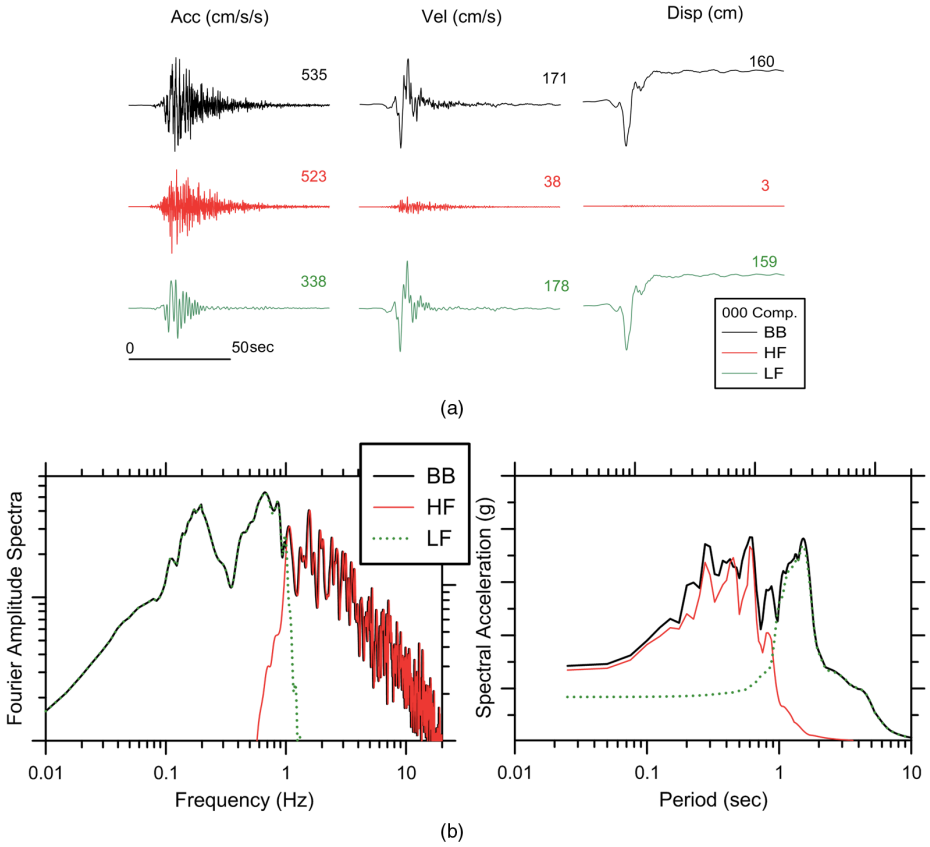

Figure 1. (a) Acceleration, velocity, and displacement histories generated for M_w 7.8 ShakeOut event at a site about 5 km from the San Andreas Fault. Results from the high-frequency (HF) and low-frequency (LF) simulations are shown along with the full broadband (BB) motions; the numbers indicate peak values. (b) Fourier amplitude spectra and 5% damped response spectra of BB, HF, and LF acceleration histories in (a). From Seyhan et al (2013).

References

Boore, D. M., J. P. Stewart, E Seyhan, G. M. Atkinson (2014). NGA-West2 Equations for Predicting PGA, PGV, and 5% Damped PSA for Shallow Crustal Earthquakes, EQ Spectra, 30(3), 1057–1085.

Boore, D. (2009). Comparing stochastic point-source and finite-source ground motion simulations:SMSIM and EXSIM, Bull. Seism. Soc. Am., 99, 3202-3216.

Campbell, K. W., and Y. Bozorgnia (2014), NGA-West2 Ground Motion Model for the Average Horizontal Components of PGA , PGV , and 5 % -Damped Linear Acceleration Response Spectra, Earthq. Spectra, 30(3), 1087–1115, doi:10.1193/062913EQS175M.

Frankel, A. (1995). Simulating strong motions of large earthquakes using recordings of small earthquakes: the Loma Prieta mainshock as a test case, Bull. Seism. Soc. Am., 85, 1144–1160.

Frankel, A. (2009). A constant stress-drop model for producing broadband synthetic seismograms: Comparison with the Next Generation Attenuation relations, Bull. Seism. Soc. Am., 99, 664-680.

Graves, R., and A. Pitarka (2016). Kinematic ground motion simulations on rough faults including effects of 3D Stochastic velocity perturbations, Bull Seis. Soc Am. 106 2136–2153.

Hillers, G., and S. G. Wesnousky (2008). Scaling relations of strike-slip earthquakes with different slip-rate dependent properties, Bull Seismol. Soc. Am. 98, 1085–1101.

Kagawa, T., K. Irikura, and P. Somerville (2004). Differences in ground motion and fault rupture process between surface and buried rupture earthquakes, Earth Planets Space 56, 3–14.

Liu, P., R. Archuleta, and S. H. Hartzell (2006). Prediction of broadband ground motion time histories: Frequency method with correlation random source parameters, Bull. Seismol. Soc. Am. 96, 2118–2130.

Mai, P. M., and G. C. Beroza (2002). A spatial random field model to characterize complexity in earthquake slip, J. Geophys. Res. 107, no. B11, 2308, doi 10.1029/2001JB000588.

Mikumo, Y. (1992). Dynamic fault rupture and stress recovery process in continental crust under depth-dependent shear strength and frictional parameters, Tectonophysics, 211, 201-222.

Pitarka, A., L. A. Dalguer, S. M. Day, P. G. Somerville, and K. Dan (2009). Numerical study of ground-motion differences between buried-rupturing and surface-rupturing earthquakes, Bull. Seismol. Soc. Am. 99, 1521-1537.

Scholz, C. (2002). The mechanics of earthquakes and faulting. Cambridge University Press.

Seyhan, E., Stewart, J. P., Graves, R. W., (2013). Calibration of a Semi-Stochastic Procedure for Simulating High-Frequency Ground Motions, Earthquake Spectra, 29, 1495-1519.

Shearer, P. M., G. A. Prieto and E. Hauksson (2006). Comprehensive analysis of earthquake source spectra in southern California, J. Geophys. Res. 111, B06303, doi:10.1029/2005JB003979.

Somerville, P., K. Irikura, R. Graves, S. Sawada, D. J. Wald, N. Abrahmason, Y. Iwasaki, T. Kagawa, N. Smith, and A. Kowada (1999). Characterizing crustal earthquake slip models for the prediction of strong ground motion, Seism. Res. Lett. 70, no. 1, 59–80.

Wirth, E.A., A.D. Frankel, and J.E. Vidale (2017). Evaluating a kinematic method for generating broadband ground motions for great earthquakes -- application to the 2003 Mw 8.3 Tokachi-Oki earthquake, Bull. Seism. Soc. Am., doi: 10.1785/0120170065.